

Single Shot Reversible GAN

for BCG artifact removal in simultaneous EEG-fMRI

Guang Lin, Jianhai Zhang, Yuxi Liu

Hangzhou Dianzi University, Hangzhou, China
{lindandan, jhzhang, shuixii}@hdu.edu.cn

Abstract

Simultaneous EEG-fMRI acquisition and analysis technology has been widely used in various research fields of brain science. However, how to remove the ballistocardiogram (BCG) artifacts in this scenario remains a huge challenge. Because it is impossible to obtain clean and BCG-contaminated EEG signals at the same time, BCG artifact removal is a typical unpaired signal-to-signal problem. To solve this problem, this paper proposed a new GAN training model - Single Shot Reversible GAN (SSRGAN). The model is allowing bidirectional input to better combine the characteristics of the two types of signals, instead of using two independent models for bidirectional conversion as in the past. Furthermore, the model is decomposed into multiple independent convolutional blocks with specific functions. Through additional training of the blocks, the local representation ability of the model is improved, thereby improving the overall model performance. Experimental results show that, compared with existing methods, the method proposed in this paper can remove BCG artifacts more effectively and retain the useful EEG information.

Single Shot Reversible GAN

Simultaneous electroencephalography (EEG) and functional magnetic resonance imaging (fMRI) acquisition provide both high temporal and spatial resolution when measuring brain activity (Mulert et al. 2009). This non-invasive and safe neuroimaging technique has proven its value in clinical diagnosis and cognitive neuroscience research (Hsiao et al. 2018; Yang et al. 2018; Tong et al. 2019), such as epileptic event localization (Hosseini et al. 2020; Hur et al. 2020) and spontaneous brain rhythms (Hunyadi et al. 2019; Mash et al. 2020).

Despite many successful applications, the utility of this technique is fundamentally limited by artifacts in EEG introduced by MRI scanner, especially ballistocardiogram (BCG) artifacts. The BCG artifact is predominantly attributed to cardiac activity and blood flow inside the static magnetic field of the MR scanner. Due to the time-varying

of the BCG artifact, the removal of BCG artifacts is often more challenging than other artifacts while analyzing EEG data recorded in an MRI environment.

Lots of previous studies have focused on BCG artifact removal, with major developments in average artifact subtraction (AAS)-based methods (Allen et al. 1998; Mullinger et al. 2013, Steyrl et al. 2018), principal component analysis (PCA)-based methods (Allen et al. 2000; Niazy et al. 2005; Marino et al. 2018), and independent component analysis (ICA)-based methods (Srivastava et al. 2005; Ghaderi et al. 2010; Vanderperren et al. 2010; Wang et al. 2018). The AAS method is based on the repetitive pattern of BCG artifacts, and it generates an artifact template to subtract it from the EEG signal. In order to make the template adapt to the change of BCG artifact, the dynamic average artifact template was developed based on median-filtering or Gaussian weighted averaging (Ellingson et al. 2004; Laufs et al. 2012). Although these techniques could mitigate the lacks of original AAS, they still have a major limitation: Most AAS-based methods need a reference electrocardiogram (ECG) signal which may not always be available. PCA and ICA, representative methods of blind source separation, are used to separate the original EEG signal into different components, then identify the BCG artifact components and finally remove them. The primary challenge with these two methods is the definition of a consistent standard for artificial component selection (Leclercq et al. 2009; Liu et al. 2012): a small number of sources may leave some artifacts, whereas a large number of sources may eliminate vital EEG information. Besides, Professional hardware equipment, like carbon fiber sling, is also used to directly measure the waveform of the BCG artifacts which are then subtracted from the contaminated EEG signal. This method can fundamentally solve the problem of BCG artifacts, whereas hardware equipment also has the problem of complicated operation and long preparation time (Xia et al. 2013; Chowdhury et al. 2014; Luo et al. 2014).

In recent years, deep learning has been widely used in neuroscience and other fields, but it is rarely used to denoise EEG signals, although significant effects have been achieved in image and audio denoising (Germain et al. 2018; Purwins et al. 2019; Tian et al. 2020). Paired data-to-data problem is to learn the mapping between input data and output data using a training set of aligned data pairs. In image denoising, the dataset X is generated by adding various noises to the dataset Y, thereby creating paired training data. However, it is impossible to obtain BCG-contaminated EEG signals (X) and clean EEG signals (Y) in the same state simultaneously; and EEG signals are more complicated than images, so it is difficult to obtain the required data by adding specific noise. This shows that converting BCG-contaminated EEG signals into clean EEG signals is an unpaired signal-to-signal problem. In this paper, we use GANs (Goodfellow et al. 2014; Zhu et al. 2017) to learn how to transform a signal from the source domain X to the target domain Y without paired examples. Meanwhile, the signal-to-noise ratio of the EEG signal is extremely low, and the direct use of CycleGAN (Zhu et al. 2017), which performs well on the unpaired problem, still cannot well remove the BCG artifacts in the simultaneous EEG-fMRI.

In response to the above problems, this paper proposes a new GAN model, called Single Shot Reversible Generative Adversarial Network (SSRGAN) which has made the following three improvements:

- Using convolution and the corresponding transposed convolution operation creates a single shot network capable of bidirectional input. The forward input can achieve data conversion from contaminated EEG signals to clean EEG signals, and the reverse input can achieve data conversion from clean EEG signals to contaminated EEG signals.
- The network is decomposed into multiple independent convolutional blocks with specific functions. The sub-network formed by combining multiple convolutional blocks is trained to improve the local representation ability of the network, thereby improving the overall performance of the network.
- The original data and the denoised data have similar features at Middle Content Layer, which can better retain information. Although there is no downstream task in our task, such an operation can provide a good feature output for future downstream tasks.

Related work

In recent years, some studies (Yang et al. 2018; McIntosh et al. 2020) have used deep learning methods to solve similar problems. Yang et al. proposed a novel method based on deep learning network (DLN) to remove Ocular artifacts (OAs) from contaminated EEG. In the training phase,

training samples without OAs are intercepted and used to train a DLN to reconstruct the EEG signals. In the testing phase, the trained DLN is used as a filter to remove OAs from the contaminated EEG signals automatically. But only using the autoencoder to train the model, the effect is mediocre in complex tasks. James et al. presented a novel method for BCG artifact suppression using recurrent neural networks (RNNs). The EEG was recovered through the nonlinear mappings between ECG and the BCG corrupted EEG. It depends on the additional ECG reference signal, while ECG data is not always useful or complete.

Due to the emergence of GANs (Goodfellow et al. 2014), many adversarial approaches with different purposes have been developed in recent years. CycleGAN (Zhu et al. 2017) present an approach for learning to translate an image from a source domain X to a target domain Y in the absence of paired examples. Neural Module Networks (Andreas et al. 2016) provides a general architecture that discretely composes neural modules into deep networks. Modular Generative Adversarial Networks (Zhao et al. 2018) is a variant based on GAN and NMN. Specific modules are responsible for specific subtasks. For example, in facial attribute transfer, specific modules are used to generate specific parts, such as glasses, mouth, and eyebrows. In the testing phase, a multi-functional network model is realized by combining multiple modules. The concept of modules is also mentioned in the paper, which we call blocks. In our work, the network is decomposed to make the network better trained, rather than combining blocks to make the network have more functions.

Single Shot Reversible GAN

This paper proposed a new GAN training model - SSRGAN. The idea of SSRGAN is not limited to GAN, it can also be applied to other deep networks. We share our code online for further research and experimentation.

Network structure

This method decomposes network into multiple independent blocks with specific functions, through which multiple sub-networks can be constructed for different tasks. It should be noted that the task here is not a sub-task of the final task, but a different new task. The architecture of SSRGAN is shown in Figure 1.

In our work, the network is decomposed into 5 blocks, which are down-sampling block, content feature block, up-sampling block and two feature conversion blocks. Since the entire network is implemented through convolution and corresponding transposed convolution, each block can input and output bidirectionally. Assuming the function of each block according to the network and task requirements, which are shown in Figure 2. In all networks, the same type of blocks shares parameters.

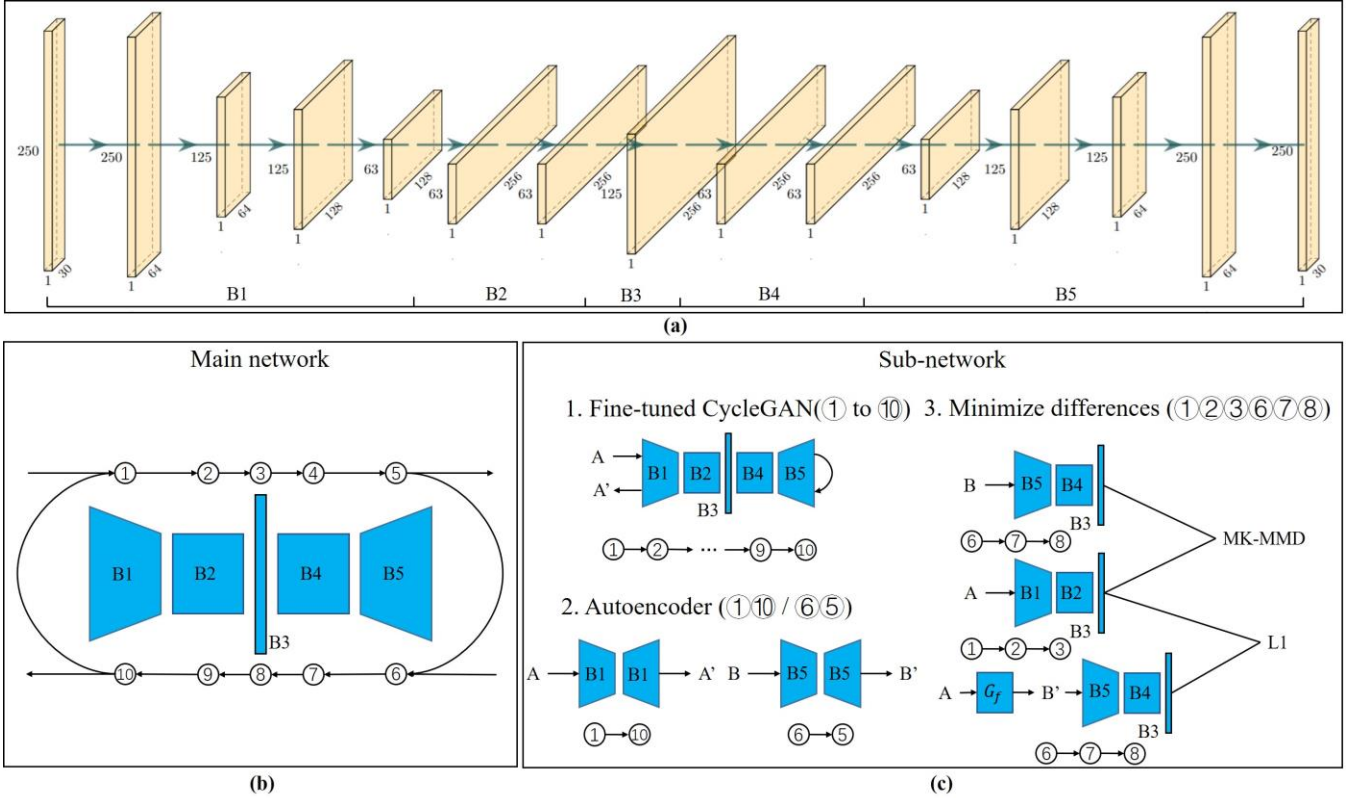


Figure 1: Model architecture and blocks. (a) Due to the large number of layers in the network, the framework of the entire network is not shown, only the convolutional layers whose feature maps have changed are displayed. (b) Numbers 1 to 10 are data flow steps, 1 to 5 are convolution operations, and 6 to 10 are the transposed convolution operations. For example, process 1: Data is input from the left, and after the convolution operation of **Block1** (B1), it is output from the right. Process 10: Data is input from the right, and after the transposed convolution operation of **Block1** (B1), it is output from the left. (c) Three sub-networks are designed for different tasks.

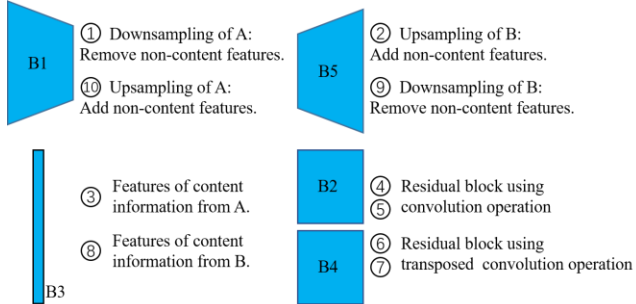


Figure 2: The functions of the blocks after training.

In theory, any number of sub-networks can be constructed by combining the blocks. According to actual task requirements, the method designs three sub-networks for removing BCG artifacts.

Fine-tuned CycleGAN

It is meaningless to use original GAN to remove BCG artifacts, even if the signal obtained is consistent with the distribution of clean EEG. Because the signal-to-noise ratio of the EEG signal is extremely low, useful information is easily

lost during the conversion process. If not adding some constraints on effectively retaining information, it is almost impossible to retain most of the useful information of the original data.

The structure of **Subnet₁** is similar to the CycleGAN structure. Under the constraint of $A = A'$, it is ensured that the information will not be excessively lost. Furthermore, two independent networks are no longer used to train two data conversion models. The convolution and the corresponding transposed convolution operation are used to construct two models. Meanwhile, parameters are shared between the two models, like a model capable of bidirectional input and output.

According to the task, two loss functions are fine-tuned in CycleGAN:

$$\mathcal{L}_{cyc}(G_f, G_r) = \mathbb{E}_{a \sim p_{data}(a)} [\| G_r(G_f(a)) - a \|_1^2] + \mathbb{E}_{b \sim p_{data}(b)} [\| G_f(G_r(b)) - b \|_1^2], \quad (1)$$

$$\mathcal{L}_{GAN}(G_f, D_B, A, B) = \mathbb{E}_{b \sim p_{data}(b)} [D_B(b)] + \mathbb{E}_{a \sim p_{data}(a)} [1 - D_B(G_f(a))]. \quad (2)$$

The G_f is the generator network obtained by the forward input model, and G_r comes from the reverse input. For each signal a from domain A , it has cycle consistency: $a \rightarrow G_f(a) \rightarrow G_r(G_f(a)) \approx a$, so does b . $\mathcal{L}_{GAN}(G_f, D_B, A, B)$ does not use log operations, which make the training more stable. D_B is the discriminator of the dataset B and discriminator D_A as well: i.e. $\mathcal{L}_{GAN}(G_r, D_A, B, A)$. The loss function of **Subnet**₁ is as follows:

$$\begin{aligned} \mathcal{L}_{sn1} = & \mathcal{L}_{cyc}(G_f, G_r) \\ & + \mathcal{L}_{GAN}(G_f, D_B, A, B) \\ & + \mathcal{L}_{GAN}(G_f, D_B, A, B), \end{aligned} \quad (3)$$

$$G_f^*, G_r^* = \min_{G_f, G_r} \max_{D_A, D_B} (\mathcal{L}_{sn1}). \quad (4)$$

Autoencoder

In the work of Yang et al., the training phase only uses the clean EEG signal for self-encoding to obtain the features of the clean data, and then the trained model is used to remove contaminated data.

Our task is relatively complicated, and autoencoder cannot completely solve such problem. Nevertheless, autoencoder can indeed extract the features of the signal very well. So, we designed **Subnet**₂ which consists of two autoencoders. As mentioned above, each block can input bidirectionally. **Block**₁ (convolution operation) and itself (corresponding transposed convolution operation) can form an autoencoder for A . Similarly, **Block**₅ can form an autoencoder for B .

The loss function of **Subnet**₂ is as follows:

$$\begin{aligned} \mathcal{L}_{sn2} = & \mathcal{L}_{AE_A}(AE_A, A) + \mathcal{L}_{AE_B}(AE_B, B) \\ = & \mathbb{E}[\|AE_A(a) - a\|_1^2] \\ & + \mathbb{E}[\|AE_B(b) - b\|_1^2]. \end{aligned} \quad (5)$$

Middle Content Layer

In order to further retain the useful information, we designed **Subnet**₃. Though making the features of Middle Content Layer similar, the useful information in the EEG signal is further retained. For the dataset A , three feature maps are output for comparison: $1 \rightarrow 2 \rightarrow 3 : \varphi_1(a)$; $6 \rightarrow 7 \rightarrow 8 : \varphi_2(a)$; $6 \rightarrow 7 \rightarrow 8 : \varphi_2(G_f(a))$. According to the data characteristics of b , a , $G_f(a)$, the loss function is as follows:

$$\begin{aligned} \mathcal{L}_{mid}(B_{1-5}, A) = & \mathcal{L}_{MSE_A}(B_{1-5}, A) + \mathcal{L}_{MKMMD_A}(B_{1-5}, A, B) \\ = & \mathbb{E}[\|\varphi_1(a) - \varphi_2(G_f(a))\|_1^2] \\ & + \mathbb{E}[\|\mathbb{E}_p[\phi_\kappa(\varphi_1(a))] - \mathbb{E}_q[\phi_\kappa(\varphi_2(b))]\|_{\mathcal{H}_\kappa}^2], \end{aligned} \quad (6)$$

where $\phi_\kappa(\cdot)$ is the corresponding mapping function associated with the kernel, and $\varphi_1(\cdot)$, $\varphi_2(\cdot)$ are $B_1(B_2(B_3(\cdot)))$, $B_5(B_4(B_3(\cdot)))$ respectively. The MK-MMD distance is defined as the distance between the average embeddings of

two probability distributions p and q in a reproducing kernel Hilbert space (RKHS) endowed with kernel κ .

The loss function of **Subnet**₃ is as follows:

$$\mathcal{L}_{sn3} = \mathcal{L}_{mid}(B_{1-5}, A) + \mathcal{L}_{mid}(B_{1-5}, B). \quad (7)$$

The original signal and the BCG-removed signal have similar features at **Block**₃, which can better retain information. Although there is no downstream task in our task, this layer can make the model an upstream task and provide a good feature output for future downstream tasks.

SSRGAN

Without the assistance of classification tasks, data denoising is more complicated. It is a challenge to keep the direction of training in line with expectations. Therefore, multiple sub-networks are trained to assist in training the main network, adding more constraints to correct the training direction. Finally, in the case of joint training, each decomposed block will gradually have the specific functions mentioned in Figure 2, thereby improving the overall network performance.

The total loss of the network is:

$$\mathcal{L}_{total} = \lambda(\mathcal{L}_{sn1} + \mathcal{L}_{sn2} + \mathcal{L}_{sn3}), \quad (8)$$

where λ is a vector used to assign weight.

Model fine-tuning

In our task, removing BCG artifacts in EEG signal noise is the most important task. So, we increase the weight of the loss function corresponding to the network of removing BCG artifacts to make the model training pay more attention to the denoising performance. According to many experiments, we modified the loss weights of multiple sub-networks to achieve the optimal network performance. In training GAN, when discriminator network is trained once, generator network is trained 2 times. This can prevent the discriminator network from converging too fast, so that the generator network cannot learn useful information. In order to further converge the generator network to obtain the best model, only the generator network is trained in the last five iterations. More details are in our code.

Dataset and Preprocessing

In this study, healthy right-handed volunteers have participated. All observers had no history of neurological disorders and gave written informed consent and paid for their participation. The study was approved by the local ethics committee.

There are two types of data used in our experiment: one is recorded in the MR scanner, the object rests in the scanner

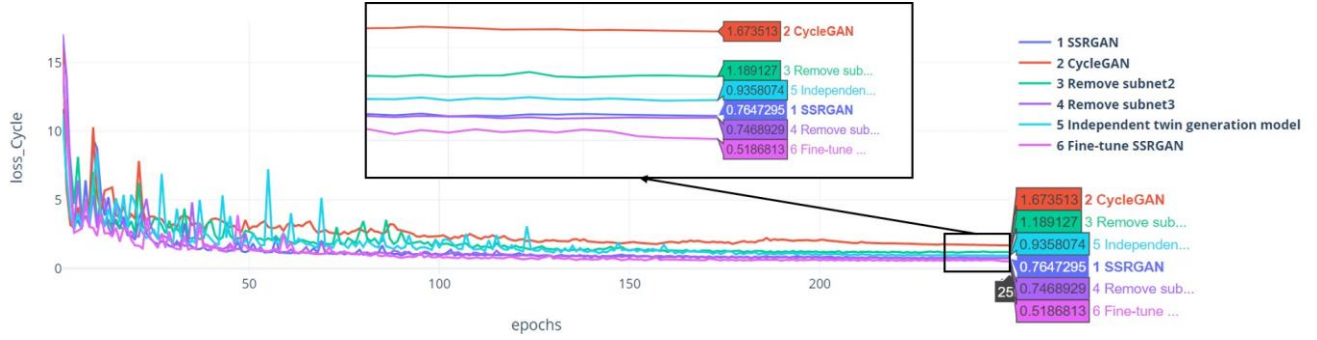


Figure 3: The loss functions of the 6 models. **Model1** is SSRGAN, and **Model2** is CycleGAN. Based on SSRGAN, **Model3, 4, 5** have been modified as follows: remove **subnet2**; remove **subnet3**; G_f and G_r no longer share parameters. **Model6** is the fine-tuned model of SSRGAN.

with the eyes open and closed, without performing any specific tasks; the other is collected under normal environmental conditions.

The trained model is tested on two subjects: DATA1: subject1 with the eyes closed; DATA2: subject1 with the eyes open; DATA3: subject2 with the eyes closed; DATA4: subject2 with the eyes open.

The EEG data were recorded using a 32-channel MR compatible EEG system consisting of 30 scalp electrodes (following the 10-20 electrode positioning system) and two additional ECG and EMG electrodes. The EEG data acquisition setup clock was synchronized with the MRI scanner clock using Brain Product's SyncBox. The sampling rate was set to 5 kHz.

For the collected data in the MR scanner, a band-pass filter from 0.1 Hz to 70 Hz is applied to remove low and high-frequency noise. The gradient artifact is removed by using FMRIB Plug-in for EEGLAB, an open-source Matlab tool. For the data collected from outside, some simple operations are used to remove eye artifacts, muscle artifacts and baseline drift. To save memory, all data were downsampled to 250Hz. Then, the processed data can be used for deep learning methods directly.

Experiments

As can be shown in Figure 3, it is proved that our method can better train the network model and make the loss further converge. The visualization results and quantification indexes are used to compare the effects of AAS-OBS, ICA, Analyzer 2 (a mature commercial software combining AAS and ICA methods) and the deep learning methods on BCG artifact removal. The results show that SSRGAN can remove BCG artifacts more effectively and retain the useful EEG information.

Loss function analysis

Among the loss functions mentioned above, Cycleloss is more representative, and is the loss function of the main network, while other loss functions serve to converge Cycleloss. Six sets of experiments are designed for comparison, and their change curve of Cycleloss are shown in Figure 3. Except for the different networks, all other strategies are consistent, such as optimizer, learning rate, batch number and other parameters. Compared with CycleGAN which is the baseline, other experiments have different improvements.

The design of **Subnet₃** did not consider the loss function to further converge, and in the experimental results, the loss did not increase after adding Middle Content Layer. So, keeping this sub-network will not reduce the performance of the model, but it can extract more useful information.

G_f and G_r sharing parameters not only can reduce the loss, but also significantly shorten the training time. Our program runs on the GPU, and the graphics card model is NVIDIA TITAN Xp 12G. When training 250 iterations, **Model₁** and **Model₅** require 5h37min and 7h25min respectively.

A variety of improvement schemes can be combined to produce different degrees of combined benefits, and that how much the network can be improved after the combination of multiple sub-networks can only be tested through experiments. In most cases, adding an adequately designed sub-network can improve performance of the overall model. After many experiments, in the task of BCG artifact removal in simultaneous EEG-fMRI, three sub-networks are selected to train the model.

Visualization

In data conversion, the up-sampling stage may also generate some noise while expanding the data. In EEG signal, most of the useful information features are concentrated in 0.1 Hz to 70 Hz. In Figure 5, the BCG-removed EEG signal (**Signal₂**) produces high-frequency noise, so we use the

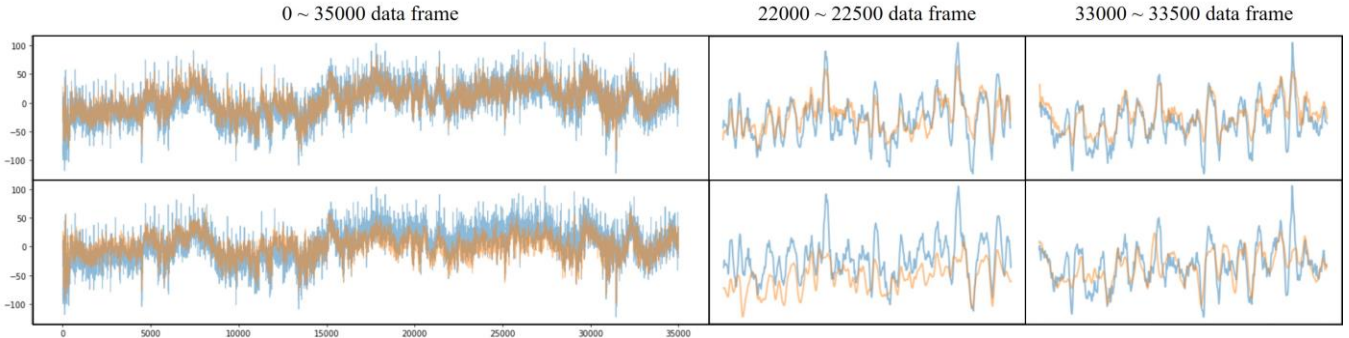


Figure 4: The upper and lower parts of the figure are our method and the results of denoising the signal using Analyzer 2. After denoising by our method, the data range is reduced, and there is no apparent shift. After using Analyzer 2 to denoise, the data range shifted.

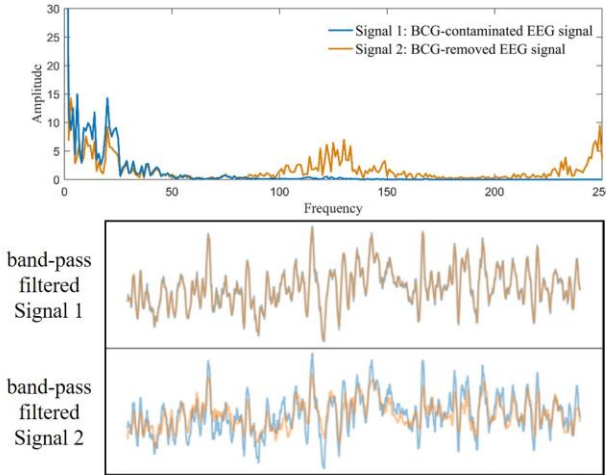


Figure 5: Spectrogram and band-pass filtered signals. The two sets of curves below the image, blue represents the BCG-contaminated signal, and orange represents the filtered curves of Signal 1 and Signal 2.

same band-pass filter with 0.1 Hz to 70 Hz as the pre-processing stage for filtering. here is almost no change in **Signal₁**, which shows that the original data remains almost unchanged after filtering; and after **Signal₂** is filtered, compared to **Signal₁**, the BCG artifacts are removed.

At present, some of the widely used commercial software use methods to locate and smooth abnormal data points based on power spectral density (PSD), peak value and other characteristics, but do not consider how to retain information better. In our method, Middle Content Layer is constructed to extract similar information from the original signal and the denoised signal and further retain the useful information. The period of BCG appearance is less than 1 second, and some studies have proved that 1 s time window is an appropriate time length in EEG signals (Wang et al. 2014). Hence, 1 s is chosen as the time window length when data segmentation. The main reason for the signal mutation in a short time is BCG. The curve changes over a long period are mainly caused by changes in the state of the subjects in

the experiment, which are useful information. As can be seen in Figure 4, our method can effectively remove BCG artifacts while retaining more useful information. There will be data drift in certain periods after using Analyzer 2 to remove BCG artifacts, which may lead to the loss of useful information.

Quantification index

One of the quantification indexes is Improvement in Normalized Power Spectral Density Ratio (INPS) (Ghaderi et al. 2010):

$$INPS = \frac{1}{n} \sum_{i=1}^n 10 \log_{10} \frac{\sum \phi_{Pbefore,i}(f)}{\sum \phi_{Pafter,i}(f)}, \quad (9)$$

where n is the number of EEG channels, and $\phi_{Pbefore,i}(\cdot)$ and $\phi_{Pafter,i}(\cdot)$ are the power spectral density of recorded EEG and cleaned EEG (i.e. after removing BCG). The EEG signals collected by synchronous EEG-fMRI contain many BCG artifacts, so the original signal energy is relatively high. Therefore, the effect of the artifact removal can be evaluated by comparing the ratio of the power spectral density of the EEG signals before and after the artifact removal. Besides, the larger value of this index shows better performance of the algorithm in terms of removing the frequency components of BCG artifact.

Another is peak-to-peak Ratio (PTPR) (Mantini et al. 2007):

$$PTPR = \frac{\frac{1}{n} \sum_{i=1}^n V_{before,i}(f)}{\frac{1}{n} \sum_{i=1}^n V_{after,i}(f)} = \frac{\sum_{i=1}^n V_{before,i}(f)}{\sum_{i=1}^n V_{after,i}(f)}, \quad (10)$$

where n is the number of EEG channels, and $V_{before,i}(\cdot)$ and $V_{after,i}(\cdot)$ are the average peak value of the channel EEG before and after the artifact. The typical amplitude of BCG is 100-1000 times that of EEG. When the peak-to-peak ratio is greater than 1, BCG artifact is removed. Again, the

		DATA1	DATA2	DATA3	DATA4
INPS	AAS-OBS	15.86	15.57	14.96	16.26
	ICA	16.48	16.72	15.61	16.61
	Analyzer 2	19.98	21.92	24.33	24.62
	CycleGAN	19.65	21.53	24.18	26.70
	Ours	20.04	21.93	24.39	24.40
PTPR	AAS-OBS	18.39	19.07	16.15	18.84
	ICA	31.36	27.86	55.86	40.40
	Analyzer 2	40.80	41.23	72.17	50.58
	Cycle GAN	31.03	30.80	60.91	50.40
	Ours	41.56	41.72	80.74	67.10

Table 1. INPS and PTPR for all subjects after removing BCG artifact

larger value of this index shows the higher ability of the algorithm to remove artifact without distorting the data.

Table 1 compares the performance of AAS-OBS, ICA, Analyzer 2, and the proposed method in terms of INPS and PTPR. Both the deep learning methods and Analyzer 2 have reached a high value in INPS. But in PTPR, only SSRGAN is better than Analyzer 2. Higher INPS and PTPR of SSRGAN can be concluded that the proposed method is obviously superior to other methods.

One limitation of AAS is that the method requires an extra ECG channel to be applicable to EEG data. Nevertheless, SSRGAN is independent on any extra signal. Besides, AAS-OBS simply believes that BCG artifacts change periodically. Based on this assumption, it will affect the accuracy of the results. In fact, the BCG is not exactly periodic. In contrast, SSRGAN does not rely on periodic behaviour for BCG that makes it robust, leading to promising results. Furthermore, compared to OBS and ICA, SSRGAN avoids the problem of artificial component selection by extracting EEG features to remove BCG artifacts. The above are the main reasons for SSRGAN to achieve improved results.

Conclusion

The removal of BCG artifacts in EEG data recorded in the MR scanner has always been a difficult problem. Based on the GAN model, this paper proposes a new training model - SSRGAN. According to experiments, this method can effectively remove BCG artifacts without data offset and can retain useful information. We hope to use Middle Content Layer to construct an upstream task to provide better features for the subsequent tasks. But without any downstream tasks, it is difficult to further prove whether the upstream task is effective. So, we plan to collect a batch of data for specific tasks in the MR scanner. The idea that improving the local representation ability of the network by training sub-networks is not limited to GAN, and can also be used in other deep networks. In the future, we will prove this in other networks and other fields (such as the image field).

References

Allen, P. J., Josephs, O., and Turner, R. 2000. A method for removing imaging artifact from continuous EEG recorded during functional MRI. *Neuroimage*, 12(2), 230-239.

Allen, P. J., Polizzi, G., Krakow, K., Fish, D. R., and Lemieux, L. 1998. Identification of EEG events in the MR scanner: the problem of pulse artifact and a method for its subtraction. *Neuroimage*, 8(3), 229-239.

Andreas, J., Rohrbach, M., Darrell, T., and Klein, D. 2016. Neural module networks. In Proceedings of the IEEE conference on computer vision and pattern recognition, 39-48

Chowdhury, M. E., Mullinger, K. J., Glover, P., and Bowtell, R. 2014. Reference layer artefact subtraction (RLAS): a novel method of minimizing EEG artefacts during simultaneous fMRI. *Neuroimage*, 84, 307-319.

Ellingson, M. L., Liebenthal, E., Spanaki, M. V., Prieto, T. E., Binder, J. R., and Ropella, K. M. 2004. Ballistocardiogram artifact reduction in the simultaneous acquisition of auditory ERPS and fMRI. *Neuroimage*, 22(4), 1534-1542.

Germain, F. G., Chen, Q., and Koltun, V. 2018. Speech denoising with deep feature losses. *arXiv preprint arXiv:1806.10522*.

Ghaderi, F., Nazarpour, K., McWhirter, J. G., & Sanei, S. 2010. Removal of ballistocardiogram artifacts using the cyclostationary source extraction method. *IEEE transactions on biomedical engineering*, 57(11), 2667-2676.

Goodfellow, I.; Pouget-Abadie, J.; Mirza, M.; Xu, B.; WardeFarley, D.; Ozair, S.; Courville, A.; and Bengio, Y. 2014. Generative adversarial nets. In *Advances in neural information processing systems*, 2672–2680.

Hosseini, M. P., Tran, T. X., Pompili, D., Elisevich, K., and Soltanian-Zadeh, H. 2020. Multimodal data analysis of epileptic EEG and rs-fMRI via deep learning and edge computing. *Artificial Intelligence in Medicine*, 104, 101813.

Hsiao, F. C., Tsai, P. J., Wu, C. W., Yang, C. M., Lane, T. J., Lee, H. C., ... and Wu, Y. Z. 2018. The neurophysiological basis of the discrepancy between objective and subjective sleep during the sleep onset period: an EEG-fMRI study. *Sleep*, 41(6), zsy056.

Hunyadi, B., Woolrich, M. W., Quinn, A. J., Vidaurre, D., and De Vos, M. 2019. A dynamic system of brain networks revealed by fast transient EEG fluctuations and their fMRI correlates. *NeuroImage*, 185, 72-82.

Hur, Y. J. 2020. Guideline for advanced neuroimaging in pediatric epilepsy. *Clinical and Experimental Pediatrics*, 63(3), 100.

Laufs, H. 2012. A personalized history of EEG-fMRI integration. *Neuroimage*, 62(2), 1056-1067.

Leclercq, Y., Balteau, E., Dang-Vu, T., Schabus, M., Luxen, A., Maquet, P., and Phillips, C. 2009. Rejection of pulse related artefact (PRA) from continuous electroencephalographic (EEG) time series recorded during functional magnetic resonance imaging (fMRI) using constraint independent component analysis (cICA). *Neuroimage*, 44(3), 679-691.

Liu, Z., de Zwart, J. A., van Gelderen, P., Kuo, L. W., and Duyn, J. H. 2012. Statistical feature extraction for artifact removal from concurrent fMRI-EEG recordings. *Neuroimage*, 59(3), 2073-2087.

Luo, Q., Huang, X., and Glover, G. H. 2014. Ballistocardiogram artifact removal with a reference layer and standard EEG cap. *Journal of neuroscience methods*, 233, 137-149.

Mantini, D., Perrucci, M. G., Cugini, S., Ferretti, A., Romani, G. L., and Del Gratta, C. 2007. Complete artifact removal for EEG recorded during continuous fMRI using independent component analysis. *Neuroimage*, 34(2), 598-607.

Marino, M., Liu, Q., Koudelka, V., Porcaro, C., Hlinka, J., Wenderoth, N., and Mantini, D. 2018. Adaptive optimal basis set for BCG artifact removal in simultaneous EEG-fMRI. *Scientific reports*, 8(1), 1-11.

Mash, L. E., Keehn, B., Linke, A. C., Liu, T. T., Helm, J. L., Haist, F., ... and Müller, R. A. 2020. Atypical relationships between spontaneous EEG and fMRI activity in autism. *Brain Connectivity*, 10(1), 18-28.

McIntosh, J. R., Yao, J., Hong, L., Faller, J., and Sajda, P. 2020. Ballistocardiogram artifact reduction in simultaneous EEG-fMRI using deep learning. *IEEE Transactions on Biomedical Engineering*.

Mulert, C., and Lemieux, L. eds. 2009. *EEG-fMRI: physiological basis, technique, and applications*. Springer Science & Business Media.

Mullinger, K. J., Havenhand, J., and Bowtell, R. 2013. Identifying the sources of the pulse artefact in EEG recordings made inside an MR scanner. *Neuroimage*, 71, 75-83.

Niazy, R. K., Beckmann, C. F., Iannetti, G. D., Brady, J. M., and Smith, S. M. 2005. Removal of fMRI environment artifacts from EEG data using optimal basis sets. *NeuroImage*, 28(3), 720-737.

Purwins, H., Li, B., Virtanen, T., Schlüter, J., Chang, S. Y., and Sainath, T. 2019. Deep learning for audio signal processing. *IEEE Journal of Selected Topics in Signal Processing*, 13(2), 206-219.

Srivastava, G., Crottaz-Herbette, S., Lau, K. M., Glover, G. H., and Menon, V. 2005. ICA-based procedures for removing ballistocardiogram artifacts from EEG data acquired in the MRI scanner. *Neuroimage*, 24(1), 50-60.

Steyrl, D., Krausz, G., Koschutnig, K., Edlinger, G., and Müller-Putz, G. R. 2018. Online reduction of artifacts in EEG of simultaneous EEG-fMRI using reference layer adaptive filtering (RLAF). *Brain topography*, 31(1), 129-149.

Tian, C., Fei, L., Zheng, W., Xu, Y., Zuo, W., and Lin, C. W. 2020. Deep learning on image denoising: An overview. *Neural Networks*.

Tong, X., An, D., Xiao, F., Lei, D., Niu, R., Li, W., ... and Zhou, B. 2019. Real-time effects of interictal spikes on hippocampus and amygdala functional connectivity in unilateral temporal lobe epilepsy: An EEG-fMRI study. *Epilepsia*, 60(2), 246-254.

Ullah, I., Hussain, M., and Aboalsamh, H. 2018. An automated system for epilepsy detection using EEG brain signals based on deep learning approach. *Expert Systems with Applications*, 107, 61-71.

Vanderperren, K., De Vos, M., Ramautar, J. R., Novitskiy, N., Mennes, M., Asseconti, S., and Lagae, L. 2010. Removal of BCG artifacts from EEG recordings inside the MR scanner: a comparison of methodological and validation-related aspects. *Neuroimage*, 50(3), 920-934.

Wang, K., Li, W., Dong, L., Zou, L., and Wang, C. 2018. Clustering-constrained ICA for ballistocardiogram artifacts removal in simultaneous EEG-fMRI. *Frontiers in neuroscience*, 12, 59.

Wang, X. W., Nie, D., and Lu, B. L. 2014. Emotional state classification from EEG data using machine learning approach. *Neurocomputing*, 129, 94-106.

Wen, T., and Zhang, Z. 2018. Deep convolution neural network and autoencoders-based unsupervised feature learning of EEG signals. *IEEE Access*, 6, 25399-25410.

Wu, X., Wu, T., Zhan, Z., Yao, L., and Wen, X. 2016. A real-time method to reduce ballistocardiogram artifacts from EEG during fMRI based on optimal basis sets (OBS). *Computer methods and programs in biomedicine*, 127, 114-125.

Xia, H., Ruan, D., and Cohen, M. S. 2013. BCG artifact removal for reconstructing full-scalp EEG inside the MR scanner. In *2013 International Workshop on Pattern Recognition in Neuroimaging* (pp. 178-181). IEEE.

Yang, B., Cao, J., Zhou, T., Dong, L., Zou, L., and Xiang, J. 2018. Exploration of neural activity under cognitive reappraisal using simultaneous EEG-fMRI data and kernel canonical correlation analysis. *Computational and mathematical methods in medicine*, 2018.

Yang, B., Duan, K., Fan, C., Hu, C., and Wang, J. 2018. Automatic ocular artifacts removal in EEG using deep learning. *Biomedical Signal Processing and Control*, 43, 148-158.

Zhao, B., Chang, B., Jie, Z., and Sigal, L. 2018. Modular generative adversarial networks. In *Proceedings of the European conference on computer vision (ECCV)*, 150-165.

Zhu, J. Y., Park, T., Isola, P., and Efros, A. A. 2017. Unpaired image-to-image translation using cycle-consistent adversarial networks. In *Proceedings of the IEEE international conference on computer vision*, 2223-2232.